Memorias del XX Congreso Latinoamericano de Control Automático (CLCA 2025)
13-17 de Octubre, 2025. Cancún, Quintana Roo, México

On the boundedness of the Coriolis matrix for robot manipulators

Julio Antonio Caballero-Mora [*,***]
Rogelio de J. Portillo-Velez [**] **Juan C. Tejada** [***]
Mario Ramirez-Neria [****]
José Alejandro Vasquez-Santacruz [**]

[*] *Faculty of Construction and Habitat, Universidad Veracruzana, Bv. Adolfo Ruíz Cortines 455, Costa Verde, Veracruz, Ver., 94294, (e-mail: jcaballeromora@gmail.com)*
[**] *Faculty of Electrical and Electronic Engineering, Universidad Veracruzana, Bv. Adolfo Ruíz Cortines 455, Costa Verde, Veracruz, Ver., 94294, (e-mail: rportillo@uv.mx, alejanvasquez@uv.mx)*
[***] *Departament of Engineering Studies for Innovation, Universidad Iberoamericana Ciudad de México, Prolongación Paseo de la Reforma 880, Colonia Lomas de Santa Fé, Ciudad de México 01219, México, (e-mail: ; juan.tejada@ibero.mx)*
[****] *InIAT Institute of Applied Research and Technology, Universidad Iberoamericana Ciudad de México, Prolongación Paseo de la Reforma 880, Colonia Lomas de Santa Fé, Ciudad de México 01219, México, (e-mail: mario.ramirez@ibero.mx)*

Abstract
Robust control design aims to alleviate uncertainties and disturbances, generally based on observers design. In this case, often it is required to know the robot dynamical model, which makes their application more complex for experimental implementations. A particular interest of this paper is to study the boundedness of the Coriolis matrix with the objective of setting conditions under which it can be neglected for the design of the controller or in the implementation of observers for robot manipulators. Theoretical conditions are proposed to bound the product $C(q,\dot{q})\dot{q}$ based on motion planning for a determined smooth Cartesian trajectory. Numerical simulations using a three degrees of freedom robot manipulator validate our findings.

Keywords: Robotics, Non-Linear Control Systems, Robot-Dynamics, Coriolis matrix, Boundedness analysis.

1. INTRODUCTION

The dynamic behavior of robotic manipulators is significantly affected by nonlinear effects such as friction and Coriolis forces, which can degrade the accuracy, stability, and responsiveness of control systems, particularly in contact-rich or high-speed manipulation tasks. Ignoring these effects may result in performance loss, instability, or inability to guarantee force tracking in precision operations Saab and Ghanem (2018); Jin et al. (2005); Eftekharian and Sayyaadi (2006). Coriolis and centrifugal forces, which are inherently velocity-dependent, introduce additional nonlinear dynamics that affect the stability and smoothness of manipulator trajectories. Although often neglected under low-velocity assumptions, it is not clear under which conditions this can be ensured. On the one hand, some research works have studied the boundedness property of the Coriolis matrix for special cases in joint space, Mulero-Martínez (2007); From et al. (2010). On the other hand, studies have shown that partial or adaptive compensation of Coriolis terms can significantly improve control performance and robustness Nagata and Watanabe (2011); Krishnamurthy et al. (2017). For instance, multivariable discrete-time controllers with partial Coriolis compensation have been shown to enhance torque regulation and trajectory tracking Saab and Ghanem (2018), while robust adaptive dynamic controllers have achieved global stabilization in manipulators under uncertain dynamics Krishnamurthy et al. (2017). The present study investigates the impact of the Coriolis term on the performance of a robot manipulator, whose dynamic model includes nonlinear effects, by analyzing the implications of conventional assumptions under which it is possible to disregard Coriolis velocity-dependent effects for a robot manipulator. Moreover, a theoretical bound that explicitly account for them is derived. The objective is to set a theoretical bound on the Coriolis term of a dynamic model of a robot manipulator with the objective to set conditions under which it can be neglected for the design of the controller or in the implementation of observers for robot manipulators, given a smooth Cartesian trajectory.

https://doi.org/10.58571/CNCA.AMCA.2025.036

The paper is organized as follows: Section 2 describes the robot's dynamic model. Section 3 presents the analysis of a theoretical bound of the Coriolis term in the dynamical model of a robot manipulator. Section 5 shows simulation results and performance evaluation. Conclusions and future directions are provided in Section 6.

2. MATHEMATICAL ROBOT MODELS

The robot direct kinematic model describes the cartesian robot positions given the robot joint positions, as in (1).

$$X = f(q) \tag{1}$$

where $X = [x, y, z, \alpha, \beta, \gamma] \in \mathbb{R}^{m\times 1}$ represents the robot posture coordinates, including the Cartesian coordinates x, y and z and the orientation angles α, β and γ; $q = [q_1, q_2, \ldots, q_n] \in \mathbb{R}^{n\times 1}$ stands for the joint variables of the robot. Moreover, the robot inverse kinematic model represents the opposite relation as given in (2); n is the dimension of the joint configuration space and m is the dimension of the cartesian space.

$$q = f^{-1}(X) \tag{2}$$

Similarly, define a mapping for Cartesian velocities $\dot{x} \in \mathbb{R}^{m\times 1}$ and joint velocities $\dot{q} \in \mathbb{R}^{n\times 1}$ as presented in (3).

$$\dot{X} = J(q)\dot{q} \tag{3}$$

where $J(q) = \frac{\partial f(q)}{\partial q} \in \mathbb{R}^{n\times m}$ represents the robot Jacobian. The dynamics of the system is affected by inertial, Coriolis, and gravitational forces; in this case we neglect frictional forces. Therefore, its motion is described by the Euler–Lagrange formulation given in (4) based on Craig (2005).

$$M(q)\ddot{q} + C(q,\dot{q})\dot{q} + G(q) = \tau, \tag{4}$$

where $M(q) \in \mathbb{R}^{n\times n}$ represents the inertia matrix, $\ddot{q} \in \mathbb{R}^{n\times 1}$ joint acceleration, $C(q,\dot{q}) \in \mathbb{R}^{n\times n}$ is the Coriolis matrix, $G(q) \in \mathbb{R}^{n\times 1}$ is the gravity vector, $\tau_c \in \mathbb{R}^{n\times 1}$ is the vector which contains the generalized torques at each actuator. All these mathematical models and parameters are known.

3. PROBLEM FORMULATION & MAIN CONTRIBUTION

To solve the problem of trajectory tracking, consider using a traditional model-based controller (Spong et al. (2006)) given in (5) for the robot dynamic model (4), where $\ddot{q}_d = [\ddot{q_{d1}}, \ddot{q_{d2}}, \ldots, \ddot{q_{dn}}] \in \mathbb{R}^{n\times 1}$ represents the joint acceleration of the desired articular trajectory to perform, $K_p \in \mathbb{R}^{n\times n}$ and $K_d \in \mathbb{R}^{n\times n}$ are diagonal matrices of proportional and derivative control gains respectively; $e = q_d - q \in \mathbb{R}^{n\times n}$ and $\dot{e} = \dot{q}_d - \dot{q} \in \mathbb{R}^{n\times n}$ are the joint tracking error and its time derivative.

$$\tau_c = M(q)(\ddot{q}_d + K_p e + K_d \dot{e}) + \alpha\, C(q,\dot{q})\dot{q} + G(q) \tag{5}$$

where α is a binary constant to study the effect of the the Coriolis term in the dynamic control of the robot manipulator. For this, this work establishes a bound on $||C(q,\dot{q})\dot{q}||$ given the Cartesian robot trajectories X, so that the Coriolis term in (5) can be neglected. This is stated in the Lemma 3.1 under the following assumptions:

- The robot manipulator has only revolute joints.
- The robot Jacobian is full rank ($n \geq m$). This also implies the robot is performing the task free of robot singularities.

Lemma 3.1. *Given a Cartesian trajectory $X(t)$ to be followed by a manipulator robot at the end-effector (EF), the bound $||C(q,\dot{q})\dot{q}|| \leq k_c \frac{||\dot{X}||^2}{\lambda_{min}(J(q)^T J(q))}$ is fulfilled along the Cartesian trajectory, where $\lambda_{min}(\cdot)$ stands for the minimum nonzero eigenvalue of $(\cdot)$).*

Proof. First, consider that the Coriolis Matrix is bounded by $||C(q,\dot{q})\dot{q}|| \leq k_c||\dot{q}||^2$, Kelly et al. (2005). Considering (3), it can be set that $||\dot{q}|| = ||J(q)^\dagger \dot{X}|| \leq ||J(q)^\dagger||\,||\dot{X}||$, where $J(q)^\dagger$ represents the Jacobian Pseudoinverse. Considering the induced norm $||J(q)^\dagger|| = \frac{1}{\sigma_{min}(J(q))}$ where $\sigma_{min}(J(q)) = \sqrt{\lambda_{min}(J(q)^T J(q))}$ stands for the minimum singular value of the Jacobian and $\lambda_{min}(\cdot)$ represents the minimum nonzero eigenvalue of $(\cdot)$; then it follows that $||\dot{q}|| = ||J(q)^\dagger \dot{X}|| \leq \frac{1}{\sigma_{min}(J(q))}||\dot{X}||$. By squaring the last expression we obtain $||\dot{q}||^2 \leq \frac{1}{\lambda_{min}(J(q)^T J(q))}||\dot{X}||^2$, we can conclude that $||C(q,\dot{q})\dot{q}|| \leq k_c \frac{||\dot{X}||^2}{\lambda_{min}(J(q)^T J(q))}$. ■

Some relevant remarks are:

(1) Note that $\lambda_{min}(J(q)^T J(q)) > 0$ provided that $J(q)^T J(q) > 0$ outside robot singularities.
(2) In the Case $n = m$, the term $J(q)^T J(q)$ is positive definite; therefore its eigenvalues are always positive. In the case of redundant robots, $n > m$; the term $J(q)^T J(q)$ is only positive semi-definite. Then, a zero eigenvalue can be found; thus the minimum nonzero eigenvalue must be chosen for $\lambda_{min}(\cdot)$.

3.1 k_c computation

According to Kelly et al. (2005), it is possible to find a positive constant k_c such that $||C(q,\dot{q})\dot{q}|| \leq k_c||\dot{q}||^2$. Having:

$$\|C_k(q)\|^2 \leq n^2 \left[\max_{i,j,q}\left\{|C_{k_{ij}}(q)|\right\}\right]^2, \tag{6}$$

where $C_{k_{ij}}(q)$ stands for the ijth element of the matrix $C_k(q)$. Then,

$$\begin{aligned}\left[\sum_{k=1}^{n}\|C_k(q)\|^2\right] &\leq n^2 \sum_{k=1}^{n}\left[\max_{i,j,q}\left\{|C_{k_{ij}}(q)|\right\}\right]^2 \\ &\leq n^3 \left[\max_{k,i,j,q}\left\{|C_{k_{ij}}(q)|\right\}\right]^2 \\ &\leq n^4 \left[\max_{k,i,j,q}\left\{|C_{k_{ij}}(q)|\right\}\right]^2 \end{aligned} \tag{7}$$

Since $n \geq 1$, is justified to maintain integer exponents. Then,

$$\|C(q,x)y\| \leq n^2 \left(\max_{k,i,j,q}|C_{k_{ij}}(q)|\right)\|x\|\|y\| \tag{8}$$

After that, it is possible to compute k_c constant as:

$$k_c = n^2 \max_{k,i,j,q}(|C_{k_{ij}}(q)|). \tag{9}$$

4. SIMULATION TESTBED

We consider a planar robotic manipulator with three revolute joints operating in the $\{x-y\}$ plane. The system is

 https://doi.org/10.58571/CNCA.AMCA.2025.036

shown in the Fig. 1 and its physical parameters are defined in Table 1.

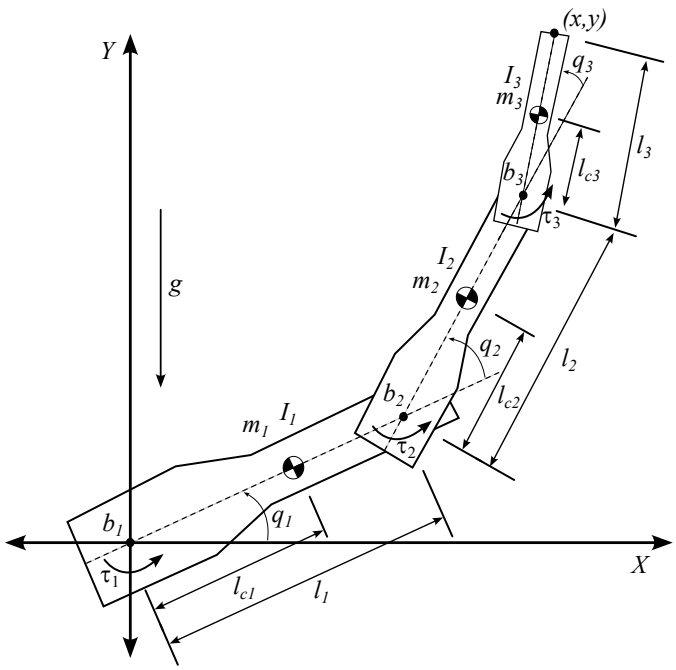

Figure 1. Scheme of 3-DOF planar robot.

4.1 Dynamic model components

To simplify the notation, we define:
$s_1 = \sin(q_1), s_{12} = \sin(q_1 + q_2), s_{123} = \sin(q_1 + q_2 + q_3)$,
$c_1 = \cos(q_1), c_{12} = \cos(q_1 + q_2), c_{123} = \cos(q_1 + q_2 + q_3)$.

Inertia matrix:

$$M(q) = \begin{bmatrix} m_{11} & m_{12} & m_{13} \\ m_{21} & m_{22} & m_{23} \\ m_{31} & m_{32} & m_{33} \end{bmatrix}, \tag{10}$$

$$\begin{aligned}
m_{11} &= I_3 + 2m_3 l_{c3} l_2 c_3 + 2m_3 l_{c3} l_1 c_{23} + m_3 l_{c3}^2 + m_2 l_1^2 \\
&\quad + m_3 l_2^2 + 2m_3 l_2 l_1 c_2 + m_3 l_1^2 + m_1 l_{c1}^2 + I_1 + I_2 \\
&\quad + 2m_2 l_{c2} l_1 c_2 + m_2 l_{c2}^2, \\
m_{12} &= I_3 + 2m_3 l_{c3} l_2 c_3 + m_3 l_{c3} l_1 c_{23} + m_3 l_{c3}^2 + m_3 l_2 l_1 c_2 \\
&\quad + m_3 l_2^2 + I_2 + m_2 l_{c2} l_1 c_2 + m_2 l_{c2}^2, \\
m_{13} &= I_3 + m_3 l_{c3}^2 + m_3 l_{c3} l_2 c_3 + m_3 l_{c3} l_1 c_{23}, \\
m_{21} &= m_{12}, \\
m_{22} &= I_2 + m_2 l_{c2}^2 + I_3 + m_3 l_{c3}^2 + 2m_3 l_{c3} l_2 c_3 + m_3 l_2^2, \\
m_{23} &= m_3 \left(l_{c3}^2 + l_{c3} l_2 c_3 \right) + I_3, \\
m_{31} &= m_{13}, \\
m_{32} &= m_{23}, \\
m_{33} &= m_3 l_{c3}^2 + I_3.
\end{aligned}$$

Coriolis and centrifugal matrix:

$$C(q, \dot{q}) = \begin{bmatrix} C_{11} & C_{12} & C_{13} \\ C_{21} & C_{22} & C_{23} \\ C_{31} & C_{32} & C_{33} \end{bmatrix}, \tag{11}$$

$$\begin{aligned}
C_{11} &= -m_2 l_{c2} l_1 s_2 \dot{q}_2 - l_1 \dot{q}_2 m_3 l_{c3} s_{23} - l_1 \dot{q}_2 m_3 l_2 s_2 \\
&\quad - m_3 l_{c3} \dot{q}_3 l_2 s_3 - m_3 l_{c3} \dot{q}_3 l_1 s_{12}, \\
C_{12} &= -m_2 l_{c2} l_1 s_2 \dot{q}_1 - l_1 m_3 l_{c3} s_{23} \dot{q}_1 - l_1 m_3 l_2 s_2 \dot{q}_1 \\
&\quad - m_2 l_{c2} l_1 s_2 \dot{q}_2 - l_1 m_3 l_{c3} s_{23} \dot{q}_2 - l_1 m_3 l_2 s_2 \dot{q}_2 \\
&\quad - m_3 l_{c3} l_2 s_3 \dot{q}_3 - m_3 l_{c3} l_1 s_{23} \dot{q}_3, \\
C_{13} &= -m_3 l_{c3} l_2 s_3 \dot{q}_1 - l_1 m_3 l_{c3} s_{23} \dot{q}_1 - m_3 l_{c3} l_2 s_3 \dot{q}_2 \\
&\quad - l_1 m_3 l_{c3} s_{23} \dot{q}_2 - m_3 l_{c3} l_2 s_3 \dot{q}_3 - m_3 l_{c3} l_1 s_{23} \dot{q}_3, \\
C_{21} &= m_2 l_{c2} l_1 s_2 \dot{q}_1 + l_1 m_3 l_{c3} s_{23} \dot{q}_1 + l_1 m_3 l_2 s_2 \dot{q}_1 \\
&\quad - m_3 l_{c3} l_2 s_3 \dot{q}_3, \\
C_{22} &= -m_3 l_{c3} l_2 s_3 \dot{q}_3, \\
C_{23} &= -m_3 l_{c3} l_2 s_3 \dot{q}_1 - m_3 l_{c3} l_2 s_3 \dot{q}_2 - m_3 l_{c3} l_2 s_3 \dot{q}_3, \\
C_{31} &= m_3 l_{c3} l_2 s_3 \dot{q}_1 + l_1 m_3 l_{c3} s_{23} \dot{q}_1 + m_3 l_{c3} l_2 s_3 \dot{q}_2, \\
C_{32} &= m_3 l_{c3} l_2 s_3 \dot{q}_1 + m_3 l_{c3} l_2 s_3 \dot{q}_2, \\
C_{33} &= 0.
\end{aligned}$$

Therefore, the $\boldsymbol{k_c}$ constant for this work is obtained as:

$$k_c = 9max\big(l_1 l_2 m_3 + l_1 l_{c2} m_2 + 2(l_1 l_{c3} m3), l_{c3} m_3 (l_2 + 2l_1)\big) \tag{12}$$

Gravity vector:

$$G(q) = \begin{bmatrix} G_1 \\ G_2 \\ G_3 \end{bmatrix}. \tag{13}$$

$$\begin{aligned}
G_1 &= m_2 g\, c_{12}\, l_{c2} + m_2 g\, c_1\, l_1 + m_1 g\, c_1\, l_{c1} \\
&\quad + m_3 g\, c_{123}\, l_{c3} + m_3 g\, c_{12}\, l_2 + m_3 g\, c_1\, l_1, \\
G_2 &= m_2 g\, c_{12}\, l_{c2} + m_3 g\, c_{123}\, l_{c3} + m_3 g\, c_{12}\, l_2, \\
G_3 &= m_3 g\, c_{123}\, l_{c3}.
\end{aligned}$$

Table 1. Physical and dynamical parameters of the 3R planar robot

Symbol	Description	Value
m_1	Mass of link 1	0.70 kg
m_2	Mass of link 2	0.60 kg
m_3	Mass of link 3	0.12 kg
l_1	Length of link 1	0.175 m
l_2	Length of link 2	0.130 m
l_3	Length of link 3	0.145 m
l_{c1}	Center of mass of link 1	0.144 m
l_{c2}	Center of mass of link 2	0.108 m
l_{c3}	Center of mass of link 3	0.060 m
I_1	Inertia of link 1	$0.016\,84\,\mathrm{kg\,m^2}$
I_2	Inertia of link 2	$0.008\,40\,\mathrm{kg\,m^2}$
I_3	Inertia of link 3	$0.000\,25\,\mathrm{kg\,m^2}$
g	Gravity acceleration	$9.81\,\mathrm{m\,s^{-2}}$

Torques $\tau = [\tau_1, \tau_2, \tau_3]^T$ are considered using the parameters of Model 2444-024B DC-Brushless Motors, which have limit: $\tau_{max} = 4.5\,\mathrm{N\,m}$.

4.2 Kinematic model

The forward kinematics map the joint configuration $q = [q_1, q_2, q_3]^T$ to the (EF) position $X = [x, y,]^T$ in the plane:

$$x = l_1\, c_1 + l_2\, c_{12} + l_3\, c_{123}, \tag{14}$$

$$y = l_1\, s_1 + l_2\, s_{12} + l_3\, s_{123}. \tag{15}$$

The geometric Jacobian matrix $J(q) \in \mathbb{R}^{2\times 3}$, which relates joint velocities to EF velocities $\dot{X} = J(q)\dot{q}$, is given by:

 https://doi.org/10.58571/CNCA.AMCA.2025.036

$$J = \begin{bmatrix} J_{11} & J_{12} & J_{13} \\ J_{21} & J_{22} & J_{23} \end{bmatrix} \tag{16}$$

where:

$$\begin{aligned} J_{11} &= -l_1 s_1 - l_2 s_{12} - l_3 s_{123} \\ J_{12} &= -l_2 s_{12} - l_3 s_{123} \\ J_{13} &= -l_3 s_{123} \\ J_{21} &= l_1 c_1 + l_2 c_{12} + l_3 c_{123} \\ J_{22} &= l_2 c_{12} + l_3 c_{123} \\ J_{23} &= l_3 c_{123} \end{aligned}$$

4.3 Motion Planning

Consider a motion planning scheme for $X_d = [x_d, y_d]^T$ and $\dot{X}_d = [v_{x_d}, v_{y_d}]^T$. For all cases of study, a smooth parabola-like desired trajectory with continuous derivatives is proposed using a fifth-order polynomial function, such that, both $\dot{X}$ and $\ddot{X}$ are equal to 0 for initial time t_i and final-time t_f. Then for all cases, the y position for any instant of t is related to:

$$y_d = a_5 t^5 + a_4 t^4 + a_3 t^3 + a_2 t^2 + a_1 t + a_0 \tag{17}$$

and y velocity for:

$$v_{y_d} = 5a_5 t^4 + 4a_4 t^3 + 3a_3 t^2 + 2a_2 t + a_1 \tag{18}$$

where $t = \left\{ t_k = t_i + k \cdot h \;\middle|\; k \in \mathbb{Z},\ 0 \le k \le \left\lfloor \frac{t_f - t_i}{h} \right\rfloor \right\}$

Consider a planar trajectory (parabola $x(y)$) with meters as unit that: starts at $(x_0, y_0) = (0.3, 0.15)$, ends at $(x_f, y_f) = (0.3, 0.3)$, passes through an intermediate point $(x_c, y_c) = (0.34, 0.225)$, and has smooth timing in $y(t)$ using the motion planning described, it can be set:

$$x(y) = a\, y^2 + b\, y + c$$

To find the coefficients a, b and c we substitute the three given points into the parabola equation in the $\{x - y\}$ plane. Solving this system of equations it is obtained: $a = -7.111$, $b = 3.200$, $c = -0.020$.

Then, the inverse kinematics problem consists in determining the joint angles q required to reach a desired position X_d in the Cartesian plane. In this work, it was solved by using Kinematic Control (KC) according to Siciliano et al. (2009). Thus the joint motion is computed by:

$$q = \int \dot{q}\, dt = \int J^{\dagger}[\dot{X}_d - K(X - X_d)]\, dt \tag{19}$$

where $K = \mathbb{I} \in \mathbb{R}^{m \times m}$ and represents a diagonal matrix of positive Cartesian gains, KC terms were defined in Sections 2 , 3.

5. RESULTS

In this section a numerical validation of Lemma 3.1 is shown. Therefore, an EF trajectory is tested in the First Cartesian Quadrant $(x+, y+)$, bounded by the robot's work-space considering simulations with an integration time-step $h = 0.001$ s. First and third simulations depicts the performance of a dynamic controller without Coriolis terms compensation ($\alpha = 0$) performing the trajectory tracking task in 0.5 s and 2 s respectively; while in second and fourth simulations the dynamic controller (5) considers Coriolis compensation ($\alpha = 1$) performing the trajectory tracking task in 0.5 s and 2 s again. For all simulations Lemma 3.1 is evaluated and also robot EF cartesian error is depicted. Taking into account the parameters $\zeta = 1$ and $\omega_n = 10$, the gains of the controller are defined by $Kp = diag\{\omega_n^2\} \in \mathbb{R}^{3\times3}$ and $K_d = diag\{2\zeta\omega_n\} \in \mathbb{R}^{3\times3}$.

5.1 Simulation 1: Coriolis uncompensated ($\alpha = 0$, $t_f = 0.5$ s)

First, the results of a simulation performing dynamic control without Coriolis effects compensation are shown. Fig. 2 presents the numerical evaluation of Lemma 3.1 along simulation. For this, a graphic comparison is depicted, showing that $max\big(||C(q,\dot{q})\dot{q}||\big) = 1.1006$ N m (indicated by an arrow) which represents the 24.5% of maximum torque that the actuators provides. Also note that $max\big(k_c \frac{||\dot{X}||^2}{\lambda_{min}(J(q)^T J(q))}\big) = 15.9069$ N m; showing that, as a maximum value, the boundary is 12 times bigger than Coriolis.

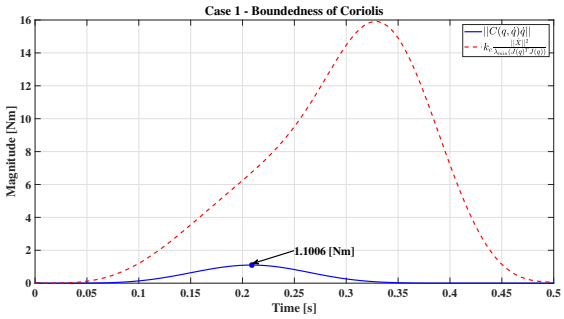

Figure 2. Case 1: Boundedness of Coriolis.

In addition, Fig. 3 depicts the cartesian errors defined as $e_x = x_d - x$ (above), and $e_y = y_d - y$ (below). From this, the max values are 0.0072 m for e_x and 0.0046 m for e_y. It physically means the robot is significantly deviating from its planned path. The performance of the robot in this simulation could be seen at **Simulation 1 - Video**.

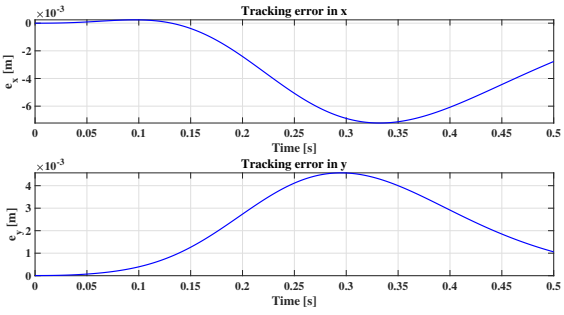

Figure 3. Case 1: Cartesian errors.

5.2 Simulation 2: Coriolis compensation ($\alpha = 1$, $t_f = 0.5$ s)

The results of dynamic controller performance considering all robot dynamics are presented here. The boundary and Coriolis values in this simulation are shown in Fig. 4, then $max\big(k_c \frac{||\dot{X}||^2}{\lambda_{min}(J(q)^T J(q))}\big) = 13.6432$ N m, 13 times higher than the maximum Coriolis value. It is also shown

 https://doi.org/10.58571/CNCA.AMCA.2025.036

$max\big(||C(q,\dot{q})\dot{q}||\big) = 1.0351\,\text{N m}$ (indicated by an arrow), which represents 23% of actuators' τ_{max}.

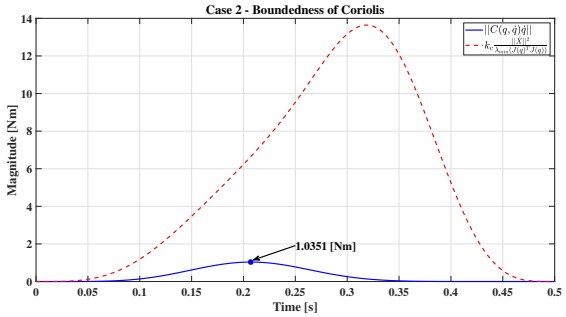

Figure 4. Case 2: Boundedness of Coriolis.

Moreover, Cartesian errors in this simulation were 9 times smaller than presented in Simulation 1, in this case, $max(e_x) = 0.0010\,\text{m}$ and $max(e_y) = 5.8557 \times 10^{-4}\,\text{m}$, as depicted in Fig. 5. Due to the error values, it is assumed that the robot's EF is almost equal to the desired path to be executed. Results of robot performance of this simulation could be seen at **Simulation 2 - Video**.

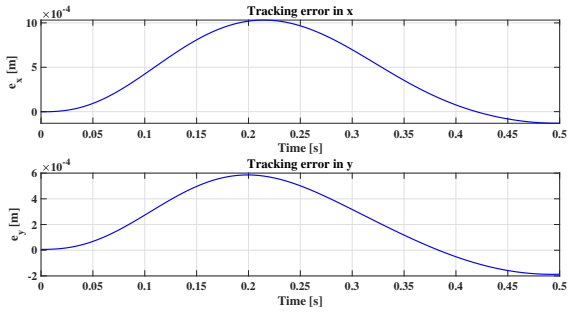

Figure 5. Case 2: Cartesian errors.

5.3 Simulation 3: Coriolis uncompensated ($\alpha = 0$, $t_f = 2\,\text{s}$)

The results for this case shows that $max\big(k_c \frac{||\dot{X}||^2}{\lambda_{min}(J(q)^T J(q))}\big) = 0.9020\,\text{N m}$, 54 times higher than the maximum Coriolis value. It is also shown $max\big(||C(q,\dot{q})\dot{q}||\big) = 0.0167\,\text{N m}$ (indicated by an arrow), which represents 0.37% of actuators' τ_{max}, as shown in Fig. 6.

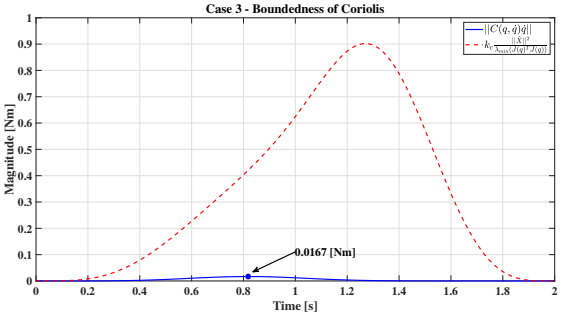

Figure 6. Case 3: Boundedness of Coriolis.

Also, the Cartesian errors are shown in Fig. 7, where $max(e_x) = 7.2234 \times 10^{-4}\,\text{m}$ and $max(e_y) = 4.1447 \times 10^{-4}\,\text{m}$. **Simulation 3 - Video** allows to see the results of robot performance of this simulation.

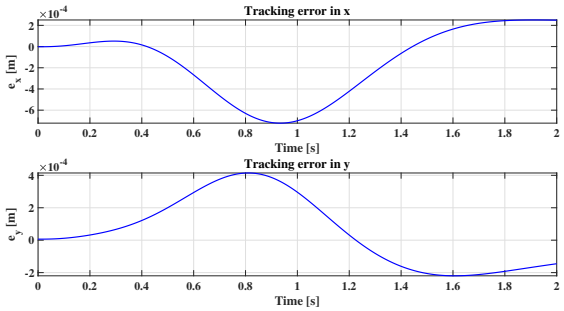

Figure 7. Case 3: Cartesian errors.

5.4 Simulation 4: Coriolis compensation ($\alpha = 1$, $t_f = 2\,\text{s}$)

Finally, in Fig. 8 is depicted that $max\big(k_c \frac{||\dot{X}||^2}{\lambda_{min}(J(q)^T J(q))}\big) = 0.8735\,\text{N m}$, 54 times higher than the maximum Coriolis value. It is also shown $max\big(||C(q,\dot{q})\dot{q}||\big) = 0.0166\,\text{N m}$ (indicated by an arrow), which represents 0.37% of actuators' τ_{max}.

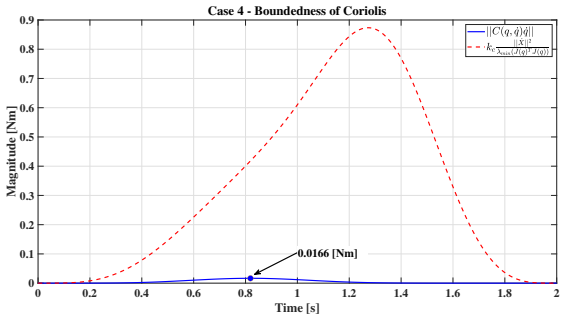

Figure 8. Case 4: Boundedness of Coriolis.

Respect to Cartesian errors, Fig. 9 indicates that $max(e_x) = 1.1912 \times 10^{-4}\,\text{m}$ and $max(e_y) = 6.6409 \times 10^{-5}\,\text{m}$. In **Simulation 4 - Video** results and robot performing are demonstrated.

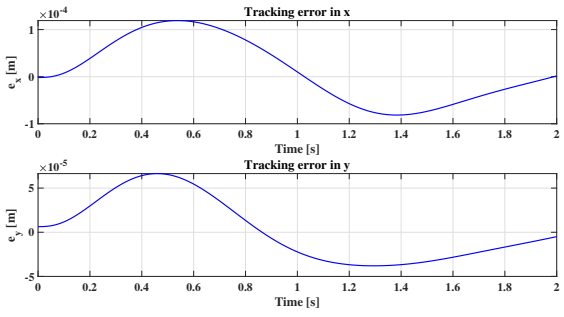

Figure 9. Case 4: Cartesian errors.

 https://doi.org/10.58571/CNCA.AMCA.2025.036

5.5 Discussion

The effectiveness of a dynamic controller is directly proportional to the fidelity of the robot's dynamic model. Based on the simulations, Coriolis term compensation significantly improves trajectory tracking. Including this term reduces the magnitude of the Coriolis effect, which is reflected in a reduction of the Cartesian errors. Neglecting terms like the Coriolis effect, even when their magnitude is small in specific configurations, introduces a systematic disturbance that degrades trajectory tracking performance. This generates significant errors in the Cartesian tracking of EF, escalating the error from negligible or millimeter-level values to magnitudes that compromise system functionality. For instance, in the 0.5 s simulations, tracking errors were reduced by ≈ 10 times when considering the robot's full dynamics. Fig. 10a clearly illustrates this improvement, showing how the compensated trajectory (X_{Case2}) aligns much better with the desired path X_d than the uncompensated one (X_{Case1}). In critical applications this deviation is not trivial, the comprehensive inclusion of all dynamic terms is fundamental for achieving optimal tracking accuracy and ensuring the robustness and reliability of the robotic system. Nonetheless, for some low-velocity robotic tasks, such as robot force control, it would be beneficial to know when is it possible to avoid Coriolis term compensation for a dynamic controller/observer. As observed, Fig. 10b depicts the same effect for the 2 s simulations, where the compensated trajectory (X_{Case4}) follows the desired path more closely than the uncompensated one (X_{Case3}). The Coriolis magnitudes are small in these cases (e.g., with a variation of just $\approx 9 \times 10^{-5}$ N m between Cases 3 and 4), including the robot's full dynamics is not essential for achieving acceptable tracking accuracy for the robot system. This shows that, in some circumstances, it is possible to neglect the Coriolis term in a dynamic controller of a robot, given a bound as the one derived in this work. Moreover, it is important to notice that the derived bound in this work is very conservative: in the simulations shown in this work it is more than 50 times the maximum Coriolis term.

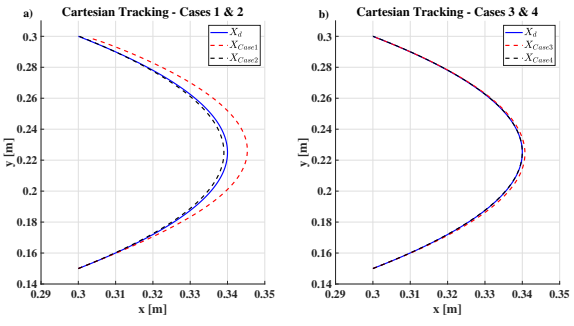

Figure 10. Cartesian trajectory tracking in simulations: (a) Cases 1&2, and Cases 3&4 in (b).

6. CONCLUSION

In this work, a bound of the Coriolis term of the dynamical model of a robot manipulator, based on the cartesian robot end effector velocity and robot Jacobian, is set. The theoretical bound has been numerically validated using standard Cartesian trajectories for a three degrees of freedom planar robot manipulator, using a model-based controller to identify the impact of the Coriolis term on its tracking performance. This result might be helpful to justify why we avoid the use of the Coriolis term in the design of robust controllers and observers. As future work we will study less conservative bounds by exploring other Matrix norms of the robot Jacobian. Also it is relevant to test our findings in an experimental testbed. Finally, the derived bound herein can be used for multiobjective trajectory planning for robot manipulators.

7. ACKNOWLEDGMENTS

The authors express their gratitude to SECIHTI for the grants assigned to Julio A. Caballero-Mora (CVU No. 809071) and Juan C. Tejada (No. 1228748); to COVE-ICYDET Veracruz for the support provided to Rogelio de J. Portillo-Velez; to InIAT for the support to Mario Ramírez-Neria; to Universidad Iberoamericana CDMX for supporting the first, third, and fourth authors; and to Universidad Veracruzana for the support given to Julio A. Caballero-Mora and Rogelio de J. Portillo-Velez.

REFERENCES

Craig, J.J. (2005). *Introduction to Robotics: Mechanics and Control*. Pearson Prentice Hall, Upper Saddle River, NJ, 3rd edition.

Eftekharian, A.A. and Sayyaadi, H. (2006). Design of mixed fuzzy-ga controller for scara type robot. 2173 – 2178.

From, P.J., Schjølberg, I., Gravdahl, J.T., Pettersen, K.Y., and Fossen, T.I. (2010). On the boundedness and skew-symmetric properties of the inertia and coriolis matrices for vehicle-manipulator systems. *IFAC Proceedings Volumes*, 43(16), 193–198. 7th IFAC Symposium on Intelligent Aut. Vehicles.

Jin, M., Kang, S.H., Chang, P.H., and Lee, E. (2005). Nonlinear bang-bang impact control: A seamless control in all contact modes. volume 2005, 557 – 564.

Kelly, R., Victor, S., and Antonio, L. (2005). *Control of Robot Manipulators in Joint Space*. Springer, London.

Krishnamurthy, P., Khorrami, F., and Wang, Z. (2017). *Robust adaptive nonlinear control for robotic manipulators with flexible joints*.

Mulero-Martínez, J.I. (2007). Uniform bounds of the coriolis/centripetal matrix of serial robot manipulators. *IEEE Trans. on Robotics*, 23(5), 1083–1089.

Nagata, F. and Watanabe, K. (2011). Adaptive learning with large variability of teaching signals for neural networks and its application to motion control of an industrial robot. *Int. Journal of Automation and Computing*, 8(1), 54 – 61.

Saab, S.S. and Ghanem, P. (2018). A multivariable stochastic tracking controller for robot manipulators without joint velocities. *IEEE Trans. on Automatic Control*, 63(8), 2481 – 2495.

Siciliano, B., Sciavicco, L., Villani, L., and Oriolo, G. (2009). *Robotics: modelling, planning and control*. Springer.

Spong, M.W., Hutchinson, S., and Vidyasagar, M. (2006). *Robot Modeling and Control*. John Wiley & Sons, Hoboken, NJ.

 https://doi.org/10.58571/CNCA.AMCA.2025.036